

Search for the decay $B^0 \rightarrow K_S^0 K_S^0 K_L^0$

B. Aubert,¹ R. Barate,¹ M. Bona,¹ D. Boutigny,¹ F. Couderc,¹ Y. Karyotakis,¹ J. P. Lees,¹ V. Poireau,¹
 V. Tisserand,¹ A. Zghiche,¹ E. Grauges,² A. Palano,³ J. C. Chen,⁴ N. D. Qi,⁴ G. Rong,⁴ P. Wang,⁴ Y. S. Zhu,⁴
 G. Eigen,⁵ I. Ofte,⁵ B. Stugu,⁵ G. S. Abrams,⁶ M. Battaglia,⁶ D. N. Brown,⁶ J. Button-Shafer,⁶ R. N. Cahn,⁶
 E. Charles,⁶ M. S. Gill,⁶ Y. Groysman,⁶ R. G. Jacobsen,⁶ J. A. Kadyk,⁶ L. T. Kerth,⁶ Yu. G. Kolomensky,⁶
 G. Kukartsev,⁶ G. Lynch,⁶ L. M. Mir,⁶ P. J. Oddone,⁶ T. J. Orimoto,⁶ M. Pripstein,⁶ N. A. Roe,⁶ M. T. Ronan,⁶
 W. A. Wenzel,⁶ P. del Amo Sanchez,⁷ M. Barrett,⁷ K. E. Ford,⁷ T. J. Harrison,⁷ A. J. Hart,⁷ C. M. Hawkes,⁷
 S. E. Morgan,⁷ A. T. Watson,⁷ K. Goetzen,⁸ T. Held,⁸ H. Koch,⁸ B. Lewandowski,⁸ M. Pelizaeus,⁸ K. Peters,⁸
 T. Schroeder,⁸ M. Steinke,⁸ J. T. Boyd,⁹ J. P. Burke,⁹ W. N. Cottingham,⁹ D. Walker,⁹ T. Cuhadar-Donszelmann,¹⁰
 B. G. Fulsom,¹⁰ C. Hearty,¹⁰ N. S. Knecht,¹⁰ T. S. Mattison,¹⁰ J. A. McKenna,¹⁰ A. Khan,¹¹ P. Kyberd,¹¹
 M. Saleem,¹¹ D. J. Sherwood,¹¹ L. Teodorescu,¹¹ V. E. Blinov,¹² A. D. Bukin,¹² V. P. Druzhinin,¹² V. B. Golubev,¹²
 A. P. Onuchin,¹² S. I. Serednyakov,¹² Yu. I. Skovpen,¹² E. P. Solodov,¹² K. Yu Todyshev,¹² D. S. Best,¹³
 M. Bondioli,¹³ M. Bruinsma,¹³ M. Chao,¹³ S. Curry,¹³ I. Eschrich,¹³ D. Kirkby,¹³ A. J. Lankford,¹³ P. Lund,¹³
 M. Mandelkern,¹³ R. K. Mommsen,¹³ W. Roethel,¹³ D. P. Stoker,¹³ S. Abachi,¹⁴ C. Buchanan,¹⁴ S. D. Foulkes,¹⁵
 J. W. Gary,¹⁵ O. Long,¹⁵ B. C. Shen,¹⁵ K. Wang,¹⁵ L. Zhang,¹⁵ H. K. Hadavand,¹⁶ E. J. Hill,¹⁶ H. P. Paar,¹⁶
 S. Rahatlou,¹⁶ V. Sharma,¹⁶ J. W. Berryhill,¹⁷ C. Campagnari,¹⁷ A. Cunha,¹⁷ B. Dahmes,¹⁷ T. M. Hong,¹⁷
 D. Kovalskiy,¹⁷ J. D. Richman,¹⁷ T. W. Beck,¹⁸ A. M. Eisner,¹⁸ C. J. Flacco,¹⁸ C. A. Heusch,¹⁸ J. Kroseberg,¹⁸
 W. S. Lockman,¹⁸ G. Nesom,¹⁸ T. Schalk,¹⁸ B. A. Schumm,¹⁸ A. Seiden,¹⁸ P. Spradlin,¹⁸ D. C. Williams,¹⁸
 M. G. Wilson,¹⁸ J. Albert,¹⁹ E. Chen,¹⁹ A. Dvoretzki,¹⁹ D. G. Hitlin,¹⁹ I. Narsky,¹⁹ T. Piatenko,¹⁹ F. C. Porter,¹⁹
 A. Ryd,¹⁹ A. Samuel,¹⁹ R. Andreassen,²⁰ G. Mancinelli,²⁰ B. T. Meadows,²⁰ M. D. Sokoloff,²⁰ F. Blanc,²¹
 P. C. Bloom,²¹ S. Chen,²¹ W. T. Ford,²¹ J. F. Hirschauer,²¹ A. Kreisel,²¹ U. Nauenberg,²¹ A. Olivas,²¹
 W. O. Ruddick,²¹ J. G. Smith,²¹ K. A. Ulmer,²¹ S. R. Wagner,²¹ J. Zhang,²¹ A. Chen,²² E. A. Eckhart,²²
 A. Soffer,²² W. H. Toki,²² R. J. Wilson,²² F. Winklmeier,²² Q. Zeng,²² D. D. Altenburg,²³ E. Feltresi,²³
 A. Hauke,²³ H. Jasper,²³ A. Petzold,²³ B. Spaan,²³ T. Brandt,²⁴ V. Klose,²⁴ H. M. Lacker,²⁴ W. F. Mader,²⁴
 R. Nogowski,²⁴ J. Schubert,²⁴ K. R. Schubert,²⁴ R. Schwierz,²⁴ J. E. Sundermann,²⁴ A. Volk,²⁴ D. Bernard,²⁵
 G. R. Bonneaud,²⁵ P. Grenier,²⁵ E. Latour,²⁵ Ch. Thiebaux,²⁵ M. Verderi,²⁵ D. J. Bard,²⁶ P. J. Clark,²⁶
 W. Gradl,²⁶ F. Muheim,²⁶ S. Playfer,²⁶ A. I. Robertson,²⁶ Y. Xie,²⁶ M. Andreotti,²⁷ D. Bettoni,²⁷ C. Bozzi,²⁷
 R. Calabrese,²⁷ G. Cibinetto,²⁷ E. Luppi,²⁷ M. Negrini,²⁷ A. Petrella,²⁷ L. Piemontese,²⁷ E. Prencipe,²⁷ F. Anulli,²⁸
 R. Baldini-Ferroli,²⁸ A. Calcaterra,²⁸ R. de Sangro,²⁸ G. Finocchiaro,²⁸ S. Pacetti,²⁸ P. Patteri,²⁸ I. M. Peruzzi,²⁸†
 M. Piccolo,²⁸ M. Rama,²⁸ A. Zallo,²⁸ A. Buzzo,²⁹ R. Capra,²⁹ R. Contri,²⁹ M. Lo Vetere,²⁹ M. M. Macri,²⁹
 M. R. Monge,²⁹ S. Passaggio,²⁹ C. Patrignani,²⁹ E. Robutti,²⁹ A. Santroni,²⁹ S. Tosi,²⁹ G. Brandenburg,³⁰
 K. S. Chaisanguanthum,³⁰ M. Morii,³⁰ J. Wu,³⁰ R. S. Dubitzky,³¹ J. Marks,³¹ S. Schenk,³¹ U. Uwer,³¹ W. Bhimji,³²
 D. A. Bowerman,³² P. D. Dauncey,³² U. Egede,³² R. L. Flack,³² J. A. Nash,³² M. B. Nikolich,³² W. Panduro
 Vazquez,³² X. Chai,³³ M. J. Charles,³³ U. Mallik,³³ N. T. Meyer,³³ V. Ziegler,³³ J. Cochran,³⁴ H. B. Crawley,³⁴
 L. Dong,³⁴ V. Eyges,³⁴ W. T. Meyer,³⁴ S. Prell,³⁴ E. I. Rosenberg,³⁴ A. E. Rubin,³⁴ A. V. Gritsan,³⁵ M. Fritsch,³⁶
 G. Schott,³⁶ N. Arnaud,³⁷ M. Davier,³⁷ G. Grosdidier,³⁷ A. Höcker,³⁷ F. Le Diberder,³⁷ V. Lepeltier,³⁷
 A. M. Lutz,³⁷ A. Oyanguren,³⁷ S. Pruvot,³⁷ S. Rodier,³⁷ P. Roudeau,³⁷ M. H. Schune,³⁷ A. Stocchi,³⁷
 W. F. Wang,³⁷ G. Wormser,³⁷ C. H. Cheng,³⁸ D. J. Lange,³⁸ D. M. Wright,³⁸ C. A. Chavez,³⁹ I. J. Forster,³⁹
 J. R. Fry,³⁹ E. Gabathuler,³⁹ R. Gamet,³⁹ K. A. George,³⁹ D. E. Hutchcroft,³⁹ D. J. Payne,³⁹ K. C. Schofield,³⁹
 C. Touramanis,³⁹ A. J. Bevan,⁴⁰ F. Di Lodovico,⁴⁰ W. Menges,⁴⁰ R. Sacco,⁴⁰ G. Cowan,⁴¹ H. U. Flaecher,⁴¹
 D. A. Hopkins,⁴¹ P. S. Jackson,⁴¹ T. R. McMahon,⁴¹ S. Ricciardi,⁴¹ F. Salvatore,⁴¹ A. C. Wren,⁴¹ D. N. Brown,⁴²
 C. L. Davis,⁴² J. Allison,⁴³ N. R. Barlow,⁴³ R. J. Barlow,⁴³ Y. M. Chia,⁴³ C. L. Edgar,⁴³ G. D. Lafferty,⁴³
 M. T. Naisbit,⁴³ J. C. Williams,⁴³ J. I. Yi,⁴³ C. Chen,⁴⁴ W. D. Hulsbergen,⁴⁴ A. Jawahery,⁴⁴ C. K. Lae,⁴⁴
 D. A. Roberts,⁴⁴ G. Simi,⁴⁴ G. Blaylock,⁴⁵ C. Dallapiccola,⁴⁵ S. S. Hertzbach,⁴⁵ X. Li,⁴⁵ T. B. Moore,⁴⁵
 S. Saremi,⁴⁵ H. Staengle,⁴⁵ S. Y. Willocq,⁴⁵ R. Cowan,⁴⁶ G. Sciolla,⁴⁶ S. J. Sekula,⁴⁶ M. Spitznagel,⁴⁶ F. Taylor,⁴⁶
 R. K. Yamamoto,⁴⁶ H. Kim,⁴⁷ P. M. Patel,⁴⁷ S. H. Robertson,⁴⁷ A. Lazzaro,⁴⁸ V. Lombardo,⁴⁸ F. Palombo,⁴⁸
 J. M. Bauer,⁴⁹ L. Cremaldi,⁴⁹ V. Eschenburg,⁴⁹ R. Godang,⁴⁹ R. Kroeger,⁴⁹ D. A. Sanders,⁴⁹ D. J. Summers,⁴⁹
 H. W. Zhao,⁴⁹ S. Brunet,⁵⁰ D. Côté,⁵⁰ P. Taras,⁵⁰ F. B. Viaud,⁵⁰ H. Nicholson,⁵¹ N. Cavallo,⁵²‡ G. De Nardo,⁵²
 F. Fabozzi,⁵²‡ C. Gatto,⁵² L. Lista,⁵² D. Monorchio,⁵² P. Paolucci,⁵² D. Piccolo,⁵² C. Sciacca,⁵² M. Baak,⁵³

G. Raven,⁵³ H. L. Snoek,⁵³ C. P. Jessop,⁵⁴ J. M. LoSecco,⁵⁴ T. Allmendinger,⁵⁵ G. Benelli,⁵⁵ K. K. Gan,⁵⁵ K. Honscheid,⁵⁵ D. Hufnagel,⁵⁵ P. D. Jackson,⁵⁵ H. Kagan,⁵⁵ R. Kass,⁵⁵ A. M. Rahimi,⁵⁵ R. Ter-Antonyan,⁵⁵ Q. K. Wong,⁵⁵ N. L. Blount,⁵⁶ J. Brau,⁵⁶ R. Frey,⁵⁶ O. Igonkina,⁵⁶ M. Lu,⁵⁶ C. T. Potter,⁵⁶ R. Rahmat,⁵⁶ N. B. Sinev,⁵⁶ D. Strom,⁵⁶ J. Strube,⁵⁶ E. Torrence,⁵⁶ F. Galeazzi,⁵⁷ A. Gaz,⁵⁷ M. Margoni,⁵⁷ M. Morandin,⁵⁷ A. Pompili,⁵⁷ M. Posocco,⁵⁷ M. Rotondo,⁵⁷ F. Simonetto,⁵⁷ R. Stroili,⁵⁷ C. Voci,⁵⁷ M. Benayoun,⁵⁸ J. Chauveau,⁵⁸ P. David,⁵⁸ L. Del Buono,⁵⁸ Ch. de la Vaissière,⁵⁸ O. Hamon,⁵⁸ B. L. Hartfiel,⁵⁸ M. J. J. John,⁵⁸ J. Malclès,⁵⁸ J. Ocariz,⁵⁸ L. Roos,⁵⁸ G. Therin,⁵⁸ P. K. Behera,⁵⁹ L. Gladney,⁵⁹ J. Panetta,⁵⁹ M. Biasini,⁶⁰ R. Covarelli,⁶⁰ M. Pioppi,⁶⁰ C. Angelini,⁶¹ G. Batignani,⁶¹ S. Bettarini,⁶¹ F. Bucci,⁶¹ G. Calderini,⁶¹ M. Carpinelli,⁶¹ R. Cenci,⁶¹ F. Forti,⁶¹ M. A. Giorgi,⁶¹ A. Lusiani,⁶¹ G. Marchiori,⁶¹ M. A. Mazur,⁶¹ M. Morganti,⁶¹ N. Neri,⁶¹ E. Paoloni,⁶¹ G. Rizzo,⁶¹ J. Walsh,⁶¹ M. Haire,⁶² D. Judd,⁶² D. E. Wagoner,⁶² J. Biesiada,⁶³ N. Danielson,⁶³ P. Elmer,⁶³ Y. P. Lau,⁶³ C. Lu,⁶³ J. Olsen,⁶³ A. J. S. Smith,⁶³ A. V. Telnov,⁶³ F. Bellini,⁶⁴ G. Cavoto,⁶⁴ A. D'Orazio,⁶⁴ D. del Re,⁶⁴ E. Di Marco,⁶⁴ R. Faccini,⁶⁴ F. Ferrarotto,⁶⁴ F. Ferroni,⁶⁴ M. Gaspero,⁶⁴ L. Li Gioi,⁶⁴ M. A. Mazzoni,⁶⁴ S. Morganti,⁶⁴ G. Piredda,⁶⁴ F. Polci,⁶⁴ F. Safai Tehrani,⁶⁴ C. Voena,⁶⁴ M. Ebert,⁶⁵ H. Schröder,⁶⁵ R. Waldi,⁶⁵ T. Adye,⁶⁶ N. De Groot,⁶⁶ B. Franek,⁶⁶ E. O. Olaiya,⁶⁶ F. F. Wilson,⁶⁶ R. Aleksan,⁶⁷ S. Emery,⁶⁷ A. Gaidot,⁶⁷ S. F. Ganzhur,⁶⁷ G. Hamel de Monchenault,⁶⁷ W. Kozanecki,⁶⁷ M. Legendre,⁶⁷ G. Vasseur,⁶⁷ Ch. Yèche,⁶⁷ M. Zito,⁶⁷ X. R. Chen,⁶⁸ H. Liu,⁶⁸ W. Park,⁶⁸ M. V. Purohit,⁶⁸ J. R. Wilson,⁶⁸ M. T. Allen,⁶⁹ D. Aston,⁶⁹ R. Bartoldus,⁶⁹ P. Bechtel,⁶⁹ N. Berger,⁶⁹ A. M. Boyarski,⁶⁹ R. Claus,⁶⁹ J. P. Coleman,⁶⁹ M. R. Convery,⁶⁹ M. Cristinziani,⁶⁹ J. C. Dingfelder,⁶⁹ J. Dorfan,⁶⁹ G. P. Dubois-Felsmann,⁶⁹ D. Dujmic,⁶⁹ W. Dunwoodie,⁶⁹ R. C. Field,⁶⁹ T. Glanzman,⁶⁹ S. J. Gowdy,⁶⁹ M. T. Graham,⁶⁹ V. Halyo,⁶⁹ C. Hast,⁶⁹ T. Hryn'ova,⁶⁹ W. R. Innes,⁶⁹ M. H. Kelsey,⁶⁹ P. Kim,⁶⁹ D. W. G. S. Leith,⁶⁹ S. Li,⁶⁹ S. Luitz,⁶⁹ V. Luth,⁶⁹ H. L. Lynch,⁶⁹ D. B. MacFarlane,⁶⁹ H. Marsiske,⁶⁹ R. Messner,⁶⁹ D. R. Muller,⁶⁹ C. P. O'Grady,⁶⁹ V. E. Ozcan,⁶⁹ A. Perazzo,⁶⁹ M. Perl,⁶⁹ T. Pulliam,⁶⁹ B. N. Ratcliff,⁶⁹ A. Roodman,⁶⁹ A. A. Salnikov,⁶⁹ R. H. Schindler,⁶⁹ J. Schwiening,⁶⁹ A. Snyder,⁶⁹ J. Stelzer,⁶⁹ D. Su,⁶⁹ M. K. Sullivan,⁶⁹ K. Suzuki,⁶⁹ S. K. Swain,⁶⁹ J. M. Thompson,⁶⁹ J. Va'vra,⁶⁹ N. van Bakel,⁶⁹ M. Weaver,⁶⁹ A. J. R. Weinstein,⁶⁹ W. J. Wisniewski,⁶⁹ M. Wittgen,⁶⁹ D. H. Wright,⁶⁹ A. K. Yarritu,⁶⁹ K. Yi,⁶⁹ C. C. Young,⁶⁹ P. R. Burchat,⁷⁰ A. J. Edwards,⁷⁰ S. A. Majewski,⁷⁰ B. A. Petersen,⁷⁰ C. Roat,⁷⁰ L. Wilden,⁷⁰ S. Ahmed,⁷¹ M. S. Alam,⁷¹ R. Bula,⁷¹ J. A. Ernst,⁷¹ V. Jain,⁷¹ B. Pan,⁷¹ M. A. Saeed,⁷¹ F. R. Wappler,⁷¹ S. B. Zain,⁷¹ W. Bugg,⁷² M. Krishnamurthy,⁷² S. M. Spanier,⁷² R. Eckmann,⁷³ J. L. Ritchie,⁷³ A. Satpathy,⁷³ C. J. Schilling,⁷³ R. F. Schwitters,⁷³ J. M. Izen,⁷⁴ I. Kitayama,⁷⁴ X. C. Lou,⁷⁴ S. Ye,⁷⁴ F. Bianchi,⁷⁵ F. Gallo,⁷⁵ D. Gamba,⁷⁵ M. Bomben,⁷⁶ L. Bosisio,⁷⁶ C. Cartaro,⁷⁶ F. Cossutti,⁷⁶ G. Della Ricca,⁷⁶ S. Dittongo,⁷⁶ S. Grancagnolo,⁷⁶ L. Lanceri,⁷⁶ L. Vitale,⁷⁶ V. Azzolini,⁷⁷ F. Martinez-Vidal,⁷⁷ Sw. Banerjee,⁷⁸ B. Bhuyan,⁷⁸ C. M. Brown,⁷⁸ D. Fortin,⁷⁸ K. Hamano,⁷⁸ R. Kowalewski,⁷⁸ I. M. Nugent,⁷⁸ J. M. Roney,⁷⁸ R. J. Sobie,⁷⁸ J. J. Back,⁷⁹ P. F. Harrison,⁷⁹ T. E. Latham,⁷⁹ G. B. Mohanty,⁷⁹ M. Pappagallo,⁷⁹ H. R. Band,⁸⁰ X. Chen,⁸⁰ B. Cheng,⁸⁰ S. Dasu,⁸⁰ M. Datta,⁸⁰ K. T. Flood,⁸⁰ J. J. Hollar,⁸⁰ P. E. Kutter,⁸⁰ B. Mellado,⁸⁰ A. Mihalys,⁸⁰ Y. Pan,⁸⁰ M. Pierini,⁸⁰ R. Prepost,⁸⁰ S. L. Wu,⁸⁰ Z. Yu,⁸⁰ and H. Neal⁸¹

(The BABAR Collaboration)

¹Laboratoire de Physique des Particules, F-74941 Annecy-le-Vieux, France

²Universitat de Barcelona, Facultat de Fisica Dept. ECM, E-08028 Barcelona, Spain

³Università di Bari, Dipartimento di Fisica and INFN, I-70126 Bari, Italy

⁴Institute of High Energy Physics, Beijing 100039, China

⁵University of Bergen, Institute of Physics, N-5007 Bergen, Norway

⁶Lawrence Berkeley National Laboratory and University of California, Berkeley, California 94720, USA

⁷University of Birmingham, Birmingham, B15 2TT, United Kingdom

⁸Ruhr Universität Bochum, Institut für Experimentalphysik 1, D-44780 Bochum, Germany

⁹University of Bristol, Bristol BS8 1TL, United Kingdom

¹⁰University of British Columbia, Vancouver, British Columbia, Canada V6T 1Z1

¹¹Brunel University, Uxbridge, Middlesex UB8 3PH, United Kingdom

¹²Budker Institute of Nuclear Physics, Novosibirsk 630090, Russia

¹³University of California at Irvine, Irvine, California 92697, USA

¹⁴University of California at Los Angeles, Los Angeles, California 90024, USA

¹⁵University of California at Riverside, Riverside, California 92521, USA

¹⁶University of California at San Diego, La Jolla, California 92093, USA

¹⁷University of California at Santa Barbara, Santa Barbara, California 93106, USA

¹⁸University of California at Santa Cruz, Institute for Particle Physics, Santa Cruz, California 95064, USA

¹⁹California Institute of Technology, Pasadena, California 91125, USA

²⁰University of Cincinnati, Cincinnati, Ohio 45221, USA

²¹University of Colorado, Boulder, Colorado 80309, USA

²²Colorado State University, Fort Collins, Colorado 80523, USA

- ²³ Universität Dortmund, Institut für Physik, D-44221 Dortmund, Germany
- ²⁴ Technische Universität Dresden, Institut für Kern- und Teilchenphysik, D-01062 Dresden, Germany
- ²⁵ Ecole Polytechnique, LLR, F-91128 Palaiseau, France
- ²⁶ University of Edinburgh, Edinburgh EH9 3JZ, United Kingdom
- ²⁷ Università di Ferrara, Dipartimento di Fisica and INFN, I-44100 Ferrara, Italy
- ²⁸ Laboratori Nazionali di Frascati dell'INFN, I-00044 Frascati, Italy
- ²⁹ Università di Genova, Dipartimento di Fisica and INFN, I-16146 Genova, Italy
- ³⁰ Harvard University, Cambridge, Massachusetts 02138, USA
- ³¹ Universität Heidelberg, Physikalisches Institut, Philosophenweg 12, D-69120 Heidelberg, Germany
- ³² Imperial College London, London, SW7 2AZ, United Kingdom
- ³³ University of Iowa, Iowa City, Iowa 52242, USA
- ³⁴ Iowa State University, Ames, Iowa 50011-3160, USA
- ³⁵ Johns Hopkins University, Baltimore, Maryland 21218, USA
- ³⁶ Universität Karlsruhe, Institut für Experimentelle Kernphysik, D-76021 Karlsruhe, Germany
- ³⁷ Laboratoire de l'Accélérateur Linéaire, IN2P3-CNRS et Université Paris-Sud 11, Centre Scientifique d'Orsay, B.P. 34, F-91898 ORSAY Cedex, France
- ³⁸ Lawrence Livermore National Laboratory, Livermore, California 94550, USA
- ³⁹ University of Liverpool, Liverpool L69 7ZE, United Kingdom
- ⁴⁰ Queen Mary, University of London, E1 4NS, United Kingdom
- ⁴¹ University of London, Royal Holloway and Bedford New College, Egham, Surrey TW20 0EX, United Kingdom
- ⁴² University of Louisville, Louisville, Kentucky 40292, USA
- ⁴³ University of Manchester, Manchester M13 9PL, United Kingdom
- ⁴⁴ University of Maryland, College Park, Maryland 20742, USA
- ⁴⁵ University of Massachusetts, Amherst, Massachusetts 01003, USA
- ⁴⁶ Massachusetts Institute of Technology, Laboratory for Nuclear Science, Cambridge, Massachusetts 02139, USA
- ⁴⁷ McGill University, Montréal, Québec, Canada H3A 2T8
- ⁴⁸ Università di Milano, Dipartimento di Fisica and INFN, I-20133 Milano, Italy
- ⁴⁹ University of Mississippi, University, Mississippi 38677, USA
- ⁵⁰ Université de Montréal, Physique des Particules, Montréal, Québec, Canada H3C 3J7
- ⁵¹ Mount Holyoke College, South Hadley, Massachusetts 01075, USA
- ⁵² Università di Napoli Federico II, Dipartimento di Scienze Fisiche and INFN, I-80126, Napoli, Italy
- ⁵³ NIKHEF, National Institute for Nuclear Physics and High Energy Physics, NL-1009 DB Amsterdam, The Netherlands
- ⁵⁴ University of Notre Dame, Notre Dame, Indiana 46556, USA
- ⁵⁵ Ohio State University, Columbus, Ohio 43210, USA
- ⁵⁶ University of Oregon, Eugene, Oregon 97403, USA
- ⁵⁷ Università di Padova, Dipartimento di Fisica and INFN, I-35131 Padova, Italy
- ⁵⁸ Universités Paris VI et VII, Laboratoire de Physique Nucléaire et de Hautes Energies, F-75252 Paris, France
- ⁵⁹ University of Pennsylvania, Philadelphia, Pennsylvania 19104, USA
- ⁶⁰ Università di Perugia, Dipartimento di Fisica and INFN, I-06100 Perugia, Italy
- ⁶¹ Università di Pisa, Dipartimento di Fisica, Scuola Normale Superiore and INFN, I-56127 Pisa, Italy
- ⁶² Prairie View A&M University, Prairie View, Texas 77446, USA
- ⁶³ Princeton University, Princeton, New Jersey 08544, USA
- ⁶⁴ Università di Roma La Sapienza, Dipartimento di Fisica and INFN, I-00185 Roma, Italy
- ⁶⁵ Universität Rostock, D-18051 Rostock, Germany
- ⁶⁶ Rutherford Appleton Laboratory, Chilton, Didcot, Oxon, OX11 0QX, United Kingdom
- ⁶⁷ DSM/Dapnia, CEA/Saclay, F-91191 Gif-sur-Yvette, France
- ⁶⁸ University of South Carolina, Columbia, South Carolina 29208, USA
- ⁶⁹ Stanford Linear Accelerator Center, Stanford, California 94309, USA
- ⁷⁰ Stanford University, Stanford, California 94305-4060, USA
- ⁷¹ State University of New York, Albany, New York 12222, USA
- ⁷² University of Tennessee, Knoxville, Tennessee 37996, USA
- ⁷³ University of Texas at Austin, Austin, Texas 78712, USA
- ⁷⁴ University of Texas at Dallas, Richardson, Texas 75083, USA
- ⁷⁵ Università di Torino, Dipartimento di Fisica Sperimentale and INFN, I-10125 Torino, Italy
- ⁷⁶ Università di Trieste, Dipartimento di Fisica and INFN, I-34127 Trieste, Italy
- ⁷⁷ IFIC, Universitat de Valencia-CSIC, E-46071 Valencia, Spain
- ⁷⁸ University of Victoria, Victoria, British Columbia, Canada V8W 3P6
- ⁷⁹ Department of Physics, University of Warwick, Coventry CV4 7AL, United Kingdom
- ⁸⁰ University of Wisconsin, Madison, Wisconsin 53706, USA
- ⁸¹ Yale University, New Haven, Connecticut 06511, USA

We present the first search for the decay $B^0 \rightarrow K_S^0 K_S^0 K_L^0$ using a data sample of 232 million $B\bar{B}$ pairs. We find no statistically significant evidence for the non-resonant component of this decay. Our central value for the branching fraction, assuming the true Dalitz distribution is uniform and

excluding the ϕ resonance, is $\mathcal{B}(B^0 \rightarrow K_s^0 K_s^0 K_L^0) = (2.4_{-2.5}^{+2.7} \pm 0.6) \times 10^{-6}$ where the errors are statistical and systematic, respectively. We set a single-sided Bayesian upper limit of $\mathcal{B}(B^0 \rightarrow K_s^0 K_s^0 K_L^0) < 7.4 \times 10^{-6}$ at 90% confidence level using a uniform prior probability for physical values. Assuming the worst-case true Dalitz distribution, where the signal is entirely in the region of lowest efficiency, the 90% confidence level upper limit is $\mathcal{B}(B^0 \rightarrow K_s^0 K_s^0 K_L^0) < 16 \times 10^{-6}$.

PACS numbers: 13.25.Hw, 12.15.Hh, 11.30.Er

I. INTRODUCTION

Measurements from the *BABAR* and Belle experiments have confirmed the Cabibbo-Kobayashi-Maskawa quark mixing matrix (CKM) mechanism [1] as the dominant source of CP violation in flavor-changing weak interactions [2]. In the Standard Model, the mixing-induced, time-dependent CP asymmetry in B^0 decays from $b \rightarrow s\bar{q}q$ penguin transitions should be the same as the precisely measured CP asymmetry in charmonium- K^0 decays, namely $\sin 2\beta$, to within a few percent. New physics from higher mass scales may contribute to the loop in the penguin diagram, which could significantly alter the CP asymmetry in penguin-dominated B decays [3]. Initial CP asymmetry measurements in $b \rightarrow s\bar{q}q$ penguin B decays have suggested a possible violation of this test of the Standard Model [4],[5],[6].

The $b \rightarrow s\bar{q}q$ penguin decays fall into two categories. If the $\bar{q}q$ can be $\bar{u}u$, a CKM-suppressed tree-level $b \rightarrow u$ transition can contribute to the decay in addition to the dominant $b \rightarrow s\bar{q}q$ penguin. This introduces some uncertainty in the Standard Model prediction of the CP asymmetry, since the $b \rightarrow u$ and the penguin amplitudes have different weak phases. On the other hand, decays such as $B^0 \rightarrow K_s^0 K_s^0 K_s^0$ [5] and $B^0 \rightarrow K_s^0 K_s^0 K_L^0$ are purely $b \rightarrow s\bar{s}s$ penguin transitions and they can only include $b \rightarrow u$ decay amplitudes through rescattering, thus the Standard Model uncertainty on the predicted CP asymmetry for these decays is generally smaller [7].

It has been noted that three-body B^0 decays of the form $B^0 \rightarrow PPP'$, where P and P' are spin-0 CP eigenstate neutral particles, are CP eigenstates[8], thus the CP asymmetry in $B^0 \rightarrow K_s^0 K_s^0 K_L^0$ is not diluted, as is generally the case in three-body B^0 decays. The $B^0 \rightarrow K_s^0 K_s^0 K_L^0$ would be a valuable addition to understanding the $b \rightarrow s\bar{q}q$ penguin CP asymmetry anomaly, if the branching fraction is large enough. The resonant ϕK_s^0 contribution to this final state, neglecting interference effects, would not yield a sample of signal events large enough to make an interesting CP asymmetry measurement. In the analysis described below, the expected and observed number of $K_s^0 K_s^0 K_L^0$ events with a $K_s^0 K_L^0$ invari-

ant mass in the region of the ϕ resonance is about eight events. Prior to our search, the non-resonant component of the $K_s^0 K_s^0 K_L^0$ final state had not been experimentally investigated. This search was motivated by the possibility of discovering a large non-resonant contribution to the $K_s^0 K_s^0 K_L^0$ final state. Large non-resonant S-wave amplitudes have been found in the Dalitz amplitude analysis of $B^+ \rightarrow K^+ K^- K^+$ [9] and $B^0 \rightarrow K^+ K^- K_s^0$ [10]. The branching fraction was recently estimated to be [7] $\mathcal{B}(B^0 \rightarrow K_s^0 K_s^0 K_L^0) = (5.23_{-1.96}^{+2.52+6.86+0.05}_{-2.53-0.06}) \times 10^{-6}$ including the ϕ resonance. The difference between the upper and lower limits of this estimate is substantial. Another prediction, based on isospin and Bose symmetry [11], gives a somewhat small branching fraction of $\mathcal{B}(B^0 \rightarrow K_s^0 K_s^0 K_L^0) = (1/3) \mathcal{B}(B^0 \rightarrow K_s^0 K_s^0 K_s^0) \approx 2 \times 10^{-6}$.

II. THE BABAR DETECTOR AND DATASET

The results presented here are based on data collected with the *BABAR* detector [12] at the PEP-II asymmetric e^+e^- collider [13] located at the Stanford Linear Accelerator Center. An integrated luminosity of 211 fb^{-1} , corresponding to $232 \times 10^6 B\bar{B}$ pairs, was recorded at the $\Upsilon(4S)$ resonance (center-of-mass energy $\sqrt{s} = 10.58 \text{ GeV}$).

Charged particles from the e^+e^- interactions are detected and their momenta are measured using five layers of double-sided silicon microstrip detectors and a 40-layer drift chamber, both operating in the 1.5-T magnetic field of a superconducting solenoid. Photons, electrons, and hadronic showers from K_L^0 interactions are identified with a CsI(Tl) electromagnetic calorimeter (EMC). Further charged particle identification is provided by the specific ionization (dE/dx) in the tracking devices and by an internally reflecting ring imaging Cherenkov detector covering the central region. The steel of the magnetic-flux return for the superconducting solenoid is instrumented with resistive plate chambers (instrumented flux return, or IFR), which are used to identify muons and hadronic showers from K_L^0 interactions.

III. ANALYSIS METHOD

A. Daughter candidate selection

We reconstruct K_s^0 candidates through the decay $K_s^0 \rightarrow \pi^+ \pi^-$ only. We begin by forming all oppositely-

*Also at Laboratoire de Physique Corpusculaire, Clermont-Ferrand, France

†Also with Università di Perugia, Dipartimento di Fisica, Perugia, Italy

‡Also with Università della Basilicata, Potenza, Italy

charged combinations of reconstructed tracks in the event. The invariant mass is required to be in the range of 490 to 506 MeV/ c^2 , assuming the tracks are pions. In addition, the χ^2 probability of the K_s^0 vertex fit must be greater than 1% and the transverse component of the decay length is required to be greater than 8 mm. Finally, the angle between the K_s^0 flight direction and the K_L^0 momentum vector must be less than 0.2 radians.

We reconstruct K_L^0 candidates by identifying clusters of energy in the EMC and hits in the IFR that are isolated from all charged tracks in the event. The K_L^0 candidates based on IFR clusters must have hits in at least two of the 16 to 19 layers in the detector. The K_L^0 candidates detected by a hadronic shower in the EMC must have a calorimeter energy of at least 200 MeV, where this energy is from interpreting the calorimeter signal as an electromagnetic shower. Clusters in the EMC that are consistent with photons from π^0 decay are vetoed by two methods. If the K_L^0 candidate EMC cluster forms an invariant mass in the range of 100 to 150 MeV/ c^2 with another EMC cluster with a calorimeter energy of at least 100 MeV, it is rejected. If the K_L^0 candidate cluster has a calorimeter energy greater than 1.0 GeV and two local maxima (or two “bumps”) in the spatial distribution of the energy within the cluster, it may be from a high-energy π^0 , where the electromagnetic showers from the two photons are merged into one cluster. If the two bumps within the cluster form an invariant mass greater than 110 MeV/ c^2 , the candidate is rejected.

Further background rejection for EMC K_L^0 candidates is achieved by using a neural network trained on signal, $q\bar{q}$ continuum (where $q = u, d, s, c$), and $B\bar{B}$ Monte Carlo samples to distinguish K_L^0 clusters from fake clusters. The neural network inputs are the EMC cluster energy and the following six shower-shape variables:

- The lateral moment LAT of the shower energy deposition [14] defined as $\text{LAT} = \sum_{i=3}^n E_i r_i^2 / (E_1 r_0^2 + E_2 r_0^2 + \sum_{i=3}^n E_i r_i^2)$ where the n crystals in the EMC cluster are ranked in order of deposited energy (E_i), $r_0 = 5$ cm is the average distance between crystal centers, and r_i is the radial distance of crystal i from the cluster center.
- The second radial moment of the shower energy deposition, defined as $\sum_i E_i r_i^2$ where r_i is the radial distance of crystal i from the cluster center.
- The energy sum of a 3×3 block of crystals, centered on the single crystal with the most energy, divided by the larger 5×5 block, also centered in the same way.
- The energy of the most energetic crystal in the cluster divided by the energy sum of the 3×3 crystal block with the most energetic crystal in the center.
- The Zernike moments [15] $A_{2,0}$ and $A_{4,2}$ defined below.

The Zernike moment $A_{n,m}$ is defined as

$$A_{n,m} = \left| \sum_i \frac{E_i}{E_{\text{tot}}} f_{n,m}(r_i/R_0) e^{im\phi_i} \right|$$

with

$$f_{2,0}(x) = 2x^2 - 1 \quad \text{and} \quad f_{4,2}(x) = 4x^4 - 3x^2$$

where r_i and ϕ_i are the radial and angular separation of crystal i with respect to the cluster center, E_{tot} is the total cluster energy, and R_0 is a cutoff radius of 15 cm. Only K_L^0 candidates that pass an optimized cut on the neural network output are retained. This cut has a signal efficiency of 85% and rejects 70% of the EMC fake K_L^0 background.

B. B^0 candidate selection

We reconstruct B^0 candidates from selected K_L^0 clusters and pairs of K_s^0 candidates that do not share any tracks. We require the sum of the K_s^0 momentum magnitudes in the center-of-mass frame to be at least 2.1 GeV/ c , which ensures consistency with the kinematics of a $B^0 \rightarrow KKK$ decay. Only the direction of the K_L^0 is reconstructed, from the vector defined by the primary vertex and the center of the neutral cluster. We compute the K_L^0 momentum by constraining the $K_s^0 K_s^0 K_L^0$ invariant mass to be the known mass of the B^0 [16]. We reject fake K_L^0 candidates by using the difference between the K_L^0 transverse momentum, computed from the B^0 mass constraint, and the transverse momentum along the K_L^0 direction that is missing from the event. The reconstructed event missing transverse momentum is calculated without using the K_L^0 cluster in the momentum sum and projected along the computed direction of the K_L^0 . This missing transverse momentum difference (reconstructed minus calculated) is required to be greater than -0.5 GeV/ c . This requirement and the previously mentioned requirement on the EMC K_L^0 neural network output were simultaneously optimized to give the greatest signal significance $S/\sqrt{S+B}$, where S and B are the expected number of signal and background events, assuming a signal branching fraction of 5×10^{-6} [7].

The difference in energy ΔE between the reconstructed B^0 candidate and the beam energy in the center-of-mass frame is the main variable used to distinguish properly reconstructed signal events from combinatoric background. The missing transverse momentum difference distributions for the signal Monte Carlo sample and the background-dominated ΔE sideband ($\Delta E > 0.010$ GeV in data) are shown in Figure 1.

We distinguish the non-resonant three-body B^0 decay from two-body B^0 decays to the same final state in this analysis. There are four two-body B^0 decays through charmonium that can go to the final state $K_s^0 K_s^0 K_L^0$, namely: $J/\psi K_s^0$, $\chi_{c0} K_L^0$, $\chi_{c2} K_L^0$, and $\psi(2S) K_s^0$. These

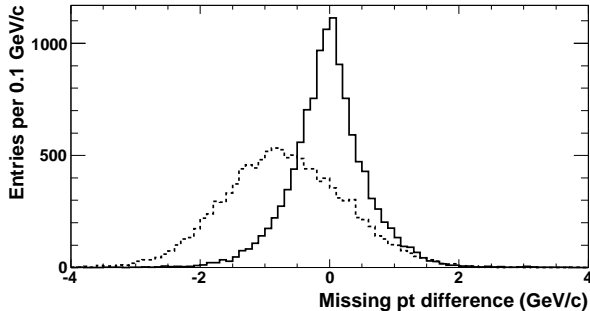


FIG. 1: Missing transverse momentum difference distributions for the signal Monte Carlo sample (solid) and the background-dominated ΔE sideband ($\Delta E > 0.010$ GeV) after all other selection criteria (see text) have been applied. The signal Monte Carlo sample distribution has been arbitrarily normalized to the number of entries in the sideband distribution.

are particularly unwanted, since they are from a color-suppressed tree decay amplitude, not the $b \rightarrow s\bar{q}q$ penguin decay amplitude. The χ_c modes have unknown B^0 branching fractions. We veto B^0 candidates consistent with $B^0 \rightarrow \chi_{c0} K_L^0$ or $B^0 \rightarrow \chi_{c2} K_L^0$, where the χ_c decays to $K_s^0 K_s^0$, by removing candidates with a $K_s^0 K_s^0$ invariant mass in the range 3.400 to 3.429 GeV/ c^2 or 3.540 to 3.585 GeV/ c^2 respectively. The combined B^0 and daughter branching fractions for the $J/\psi K_s^0$ and $\psi(2S) K_s^0$ modes are 0.062 and 0.016 times 10^{-6} respectively. We expect about two events from two-body B^0 decays through charmonium in our final sample.

We also remove B^0 candidates consistent with $B^0 \rightarrow \phi K_s^0$ with $\phi \rightarrow K_s^0 K_L^0$ by requiring the invariant mass of both $K_s^0 K_L^0$ combinations to be above 1.049 GeV/ c^2 , though as a cross check, we measure the branching fraction in only the ϕK_s^0 region, where one $K_s^0 K_L^0$ combination has an invariant mass less than 1.049 GeV/ c^2 . These two-body B^0 decay vetos are 96.6% efficient for the $B^0 \rightarrow K_s^0 K_s^0 K_L^0$ signal Monte Carlo sample generated with a uniform true Dalitz distribution.

C. Event selection

The main source of background is from random $K_s^0 K_s^0 K_L^0$ combinations from continuum $q\bar{q}$ events. We combine 3 variables in a neural network that is trained using Monte Carlo samples to distinguish signal from continuum events. The first input is the cosine of the angle of the B^0 momentum with respect to the beam axis in the center-of-mass frame θ_B^* , which is flat for continuum background whereas the signal probability is proportional to $\sin^2 \theta_B^*$. The other two inputs are topological variables that are commonly used to distinguish jet-like continuum events from the more isotropic particle distributions in $B\bar{B}$ events. The first is the cosine

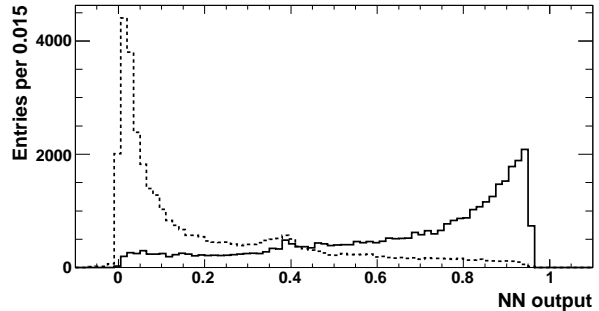


FIG. 2: Neural network output (NN) distributions for the signal Monte Carlo sample (solid) and the background-dominated ΔE sideband ($\Delta E > 0.010$ GeV) after all other selection criteria (see text) have been applied. The signal Monte Carlo sample distribution has been arbitrarily normalized to the number of entries in the sideband distribution.

of the angle θ_T between the thrust axis of the B^0 candidate in the center-of-mass frame and that of the rest of the charged tracks and neutral calorimeter clusters in the event. The distribution of $|\cos \theta_T|$ is sharply peaked near 1.0 for combinations drawn from jet-like $q\bar{q}$ pairs, and nearly uniform for B^0 meson decays. The second is a linear combination of the zeroth and second angular moments $L_{0,2}$ of the energy flow about the B^0 thrust axis. The moments are defined by $L_j = \sum_i p_i \times |\cos \theta_i|^j$, where θ_i is the angle with respect to the B^0 thrust axis of track or neutral cluster i , p_i is its momentum, and the sum excludes the B^0 candidate daughters. Distributions of the neural network output NN for the signal Monte Carlo sample and the background-dominated ΔE sideband are shown in Figure 2. We require $NN > 0.5$ to remove events that have little probability of being signal.

After all of the requirements stated thus far, if an event has more than one B^0 candidate, we choose the best one by selecting on the quality of the K_L^0 cluster. If there are one or more EMC K_L^0 candidates, the best K_L^0 candidate is the one with the highest cluster calorimeter energy. If there are no EMC K_L^0 candidates, the best K_L^0 candidate is the one with the highest number of IFR layers with hits in the K_L^0 cluster. If there is more than one K_s^0 pair that uses the same (best) K_L^0 cluster, the best B^0 candidate is the one with the lowest K_s^0 mass χ^2 , defined below

$$\chi^2 = \left(\frac{\delta m_1}{\sigma} \right)^2 + \left(\frac{\delta m_2}{\sigma} \right)^2$$

where δm_i is the difference between the reconstructed invariant mass of K_s^0 candidate i and the known K_s^0 mass [16] and σ is the invariant mass resolution (2.9 MeV/ c^2).

Our final analysis sample contains 5892 events with ΔE in the range of -0.010 GeV to 0.080 GeV. Signal events appear mostly in the range of -0.010 GeV to 0.010 GeV. The $\Delta E > 0.010$ GeV region is dominated

by combinatoric background. The signal efficiency varies from 4% to 14% depending on the position in the Dalitz plot. The signal efficiency as a function of Dalitz plot position and a histogram of the reconstruction efficiency for 322 uniformly distributed points in the Dalitz plot are shown in Figures 3 and 4 respectively. For a uniform true Dalitz distribution, the average signal efficiency is 8.1%.

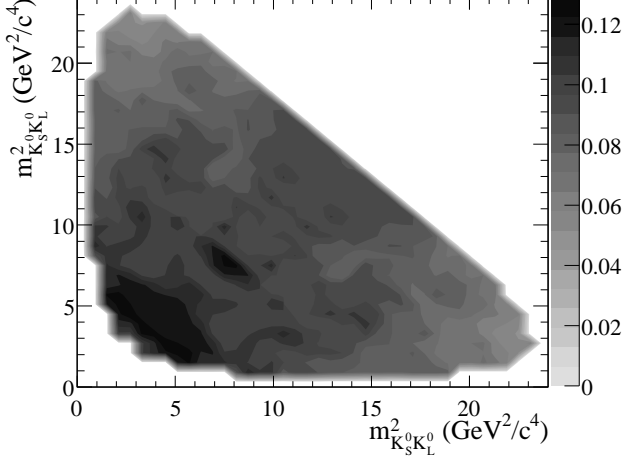


FIG. 3: The reconstruction efficiency for signal as a function of position in the symmetrized Dalitz plot.

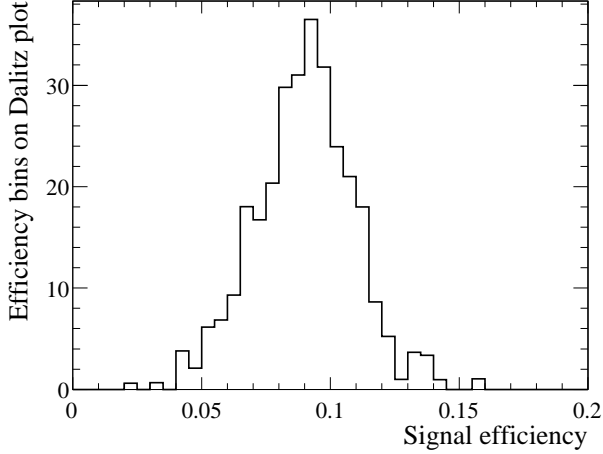


FIG. 4: A histogram of the reconstruction efficiency for signal for 322 uniformly distributed points in the Dalitz plot.

D. $J/\psi K_L^0$ control sample

We use a sample of $B^0 \rightarrow J/\psi K_L^0$ decays from the data to calibrate the reconstruction and selection efficiency and the ΔE resolution. The J/ψ is reconstructed

in the e^+e^- and $\mu^+\mu^-$ channels. We apply the same K_L^0 selection, projected missing transverse momentum difference, and NN criteria as for our $K_S^0 K_S^0 K_L^0$ selection. The ratio of the $K_S^0 K_S^0 K_L^0$ and $J/\psi K_L^0$ Monte Carlo efficiencies for these criteria is $\epsilon_{K_S^0 K_S^0 K_L^0} / \epsilon_{J/\psi K_L^0} = 0.96$. We compare the number of fitted $J/\psi K_L^0$ events to the predicted number of events, based on the known branching fractions and the Monte Carlo efficiency. The $J/\psi K_L^0$ reconstruction efficiency for all selection criteria is 12.5%. We find $N_{\text{obs}} = 1420 \pm 56$ $J/\psi K_L^0$ events, consistent with the predicted yield of $N_0 = 1426 \pm 86$. We correct the $K_S^0 K_S^0 K_L^0$ efficiency by multiplying the MC efficiency by a correction factor of 0.96 ± 0.08 , which is defined as $(N_{\text{obs}}/N_0) \times (\epsilon_{K_S^0 K_S^0 K_L^0} / \epsilon_{J/\psi K_L^0})$. The uncertainty on the correction factor includes the uncertainties on the relevant branching fractions for $J/\psi K_L^0$, the statistical error from the $J/\psi K_L^0$ fit, and our estimated uncertainty on relating the $J/\psi K_L^0$ and $K_S^0 K_S^0 K_L^0$ selection and reconstruction efficiencies.

The ΔE resolution is better for EMC candidates because the position of the hadronic shower is more precisely measured. We also use the $J/\psi K_L^0$ to measure the signal ΔE resolution separately for K_L^0 candidates reconstructed in the EMC and IFR. Figure 5 shows the fitted ΔE distributions for EMC and IFR K_L^0 candidates.

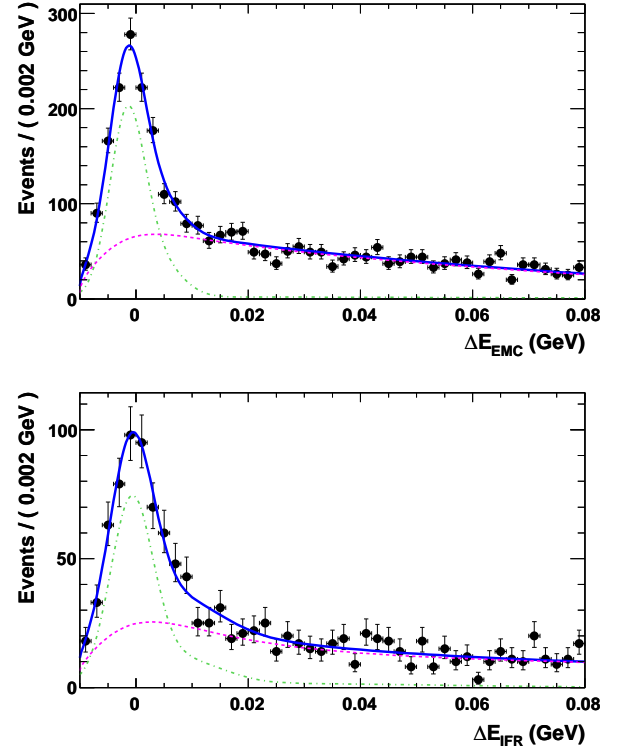


FIG. 5: Fitted ΔE distributions of the $J/\psi K_L^0$ control sample for EMC (top) and IFR (bottom) K_L^0 candidates. The points with error bars are histograms of the data sample. The solid curve is the total PDF. The dot-dashed curve is the signal PDF and the dashed curve is the background PDF.

E. Signal yield determination

We use an extended unbinned maximum likelihood fit to determine the number of signal events in our final sample. The likelihood for an event is the product of probability density functions (PDFs) for the two main discriminating variables in the analysis: ΔE and NN . Separate PDFs are used for EMC and IFR candidates due to the difference in ΔE resolution and the fact that some background channels mostly produce fake signal for EMC K_L^0 candidates only. The EMC and IFR K_L^0 samples are fitted simultaneously and the relative fraction of EMC signal events is taken from the $J/\psi K_L^0$ control sample. Separate PDFs are also used for signal, combinatoric background, and three classes of background from B decays similar to our signal (“peaking backgrounds” described below in Section III F). The combinatoric background includes random $K_s^0 K_s^0 K_L^0$ combinations from $B\bar{B}$ events as well as from continuum events.

Figure 6 shows the ΔE and NN PDFs for all five fit components. The numbers of signal and combinatoric background events are determined from the fit. The peaking background yields are fixed to values based on known and estimated branching fractions and then varied in the evaluation of systematic uncertainties.

The functional form of the signal PDF for ΔE is a triple Gaussian distribution. The mean and width of the core Gaussian distribution are determined separately for EMC and IFR K_L^0 candidates from the $J/\psi K_L^0$ control sample and held fixed in the $K_s^0 K_s^0 K_L^0$ fit. The remaining Gaussian parameters for the signal ΔE PDF are determined from the signal Monte Carlo sample and held fixed. The signal PDF for NN is a 4th-order polynomial. The polynomial coefficients are determined from the signal Monte Carlo sample and held fixed in the fit. The combinatoric background ΔE PDF is an ARGUS function [17]. The NN PDF for combinatoric background is the sum of a 1st-order polynomial and an ARGUS function. The PDF shape parameters for the combinatoric background component are free in the fit.

F. Backgrounds from other B decays

Backgrounds from B decays to final states similar to $K_s^0 K_s^0 K_L^0$ can look similar to our signal in our discriminating variables ΔE and NN . We call events from these decays “peaking backgrounds.” The largest single source of peaking background is the decay $B^0 \rightarrow K_s^0 K_s^0 K_s^0$. One of the K_s^0 can decay to $\pi^0 \pi^0$, where one or more of the photons from either π^0 fakes the K_L^0 cluster in the EMC. The world average $K_s^0 K_s^0 K_s^0$ branching fraction from the Heavy Flavor Averaging Group (HFAG)[6],[5] is $\mathcal{B}(B^0 \rightarrow K_s^0 K_s^0 K_s^0) = (6.2 \pm 0.9) \times 10^{-6}$. We expect 20 $K_s^0 K_s^0 K_s^0$ events in our fit sample and vary this number by ± 5 events in the evaluation of the systematic errors.

Decays of the type KKK^* can produce a $K_s^0 K_s^0 K_L^0 \pi$ final state, which can look similar to our signal if the

momentum of the additional π is low. The branching fractions for the relevant KKK^* have not been measured. We assume they are each of the same order as our expected signal, based on comparing the relative branching ratios of $B \rightarrow K\pi$ decays with $B \rightarrow K^*\pi$ and $B \rightarrow K\rho$ decays. We estimate a total branching fraction of 30×10^{-6} for this inclusive final state and vary this assumption by $\pm 15 \times 10^{-6}$ in the evaluation of systematic errors. This gives us an expected 70 ± 35 events from KKK^* in the fit sample. In the evaluation of the 90% C. L. upper limit on the branching fraction, we set the KKK^* event yield to zero. This is the most conservative assumption, since the signal and KKK^* event yields are anti-correlated in the fit.

Finally, the decay $B^0 \rightarrow K_s^0 K_s^0 \pi^0$ can also mimic our signal if the π^0 is misidentified as a K_L^0 in the EMC. The branching fraction for this mode has also not been measured. We estimate the branching fraction, relative to our signal, by assuming that the tree-to-penguin ratio for the three-body decays is the same as for $B^0 \rightarrow \pi^0 \pi^0$ vs $B^0 \rightarrow K^0 \pi^0$ and that our signal branching fraction is about 5×10^{-6} [7]. Our estimate for the branching fraction is $\mathcal{B}(B^0 \rightarrow K_s^0 K_s^0 \pi^0) \approx 1.6 \times 10^{-6}$ and we vary this assumed branching fraction in the range $[0.1, 5.0] \times 10^{-6}$ in the evaluation of systematic errors. This gives us an expected 2_{-2}^{+4} events from $K_s^0 K_s^0 \pi^0$ in the fit sample.

The ΔE and NN PDFs for the three peaking background components above are determined from Monte Carlo samples. In general, the ΔE shape peaks near $\Delta E = 0$, though there is a substantial tail that extends to high ΔE values. We use the sum of an ARGUS function and a Landau function for the peaking background ΔE PDF. The NN shape is quite similar to the signal shape for all three peaking backgrounds. The form of the NN PDF is a polynomial. The ΔE and NN PDFs for the three peaking background components are shown in Figure 6: c, d, and e.

IV. RESULTS

Table I lists the results of the maximum likelihood fit. We find $23_{-22}^{+23} \pm 6$ events for the $K_s^0 K_s^0 K_L^0$ signal yield, where the first errors are statistical and the second error is systematic. The maximum likelihood fit bias of $+0.3$ signal events was evaluated from an ensemble of data sets composed of fully simulated signal and B background Monte Carlo events. The combinatoric background for these datasets was generated from the PDF parameters of the fit to the data. This average bias of 0.3 events and the expected 2.1 events from B^0 decays through charmonium are subtracted from the fitted signal yield.

The systematic errors on the fitted signal yield and the signal branching fraction are listed in Table II. The additive contributions to the systematic error come from the uncertainty on our estimation of the KKK^* component normalization (5.2 events), varying the yields of the other fixed peaking background components and the

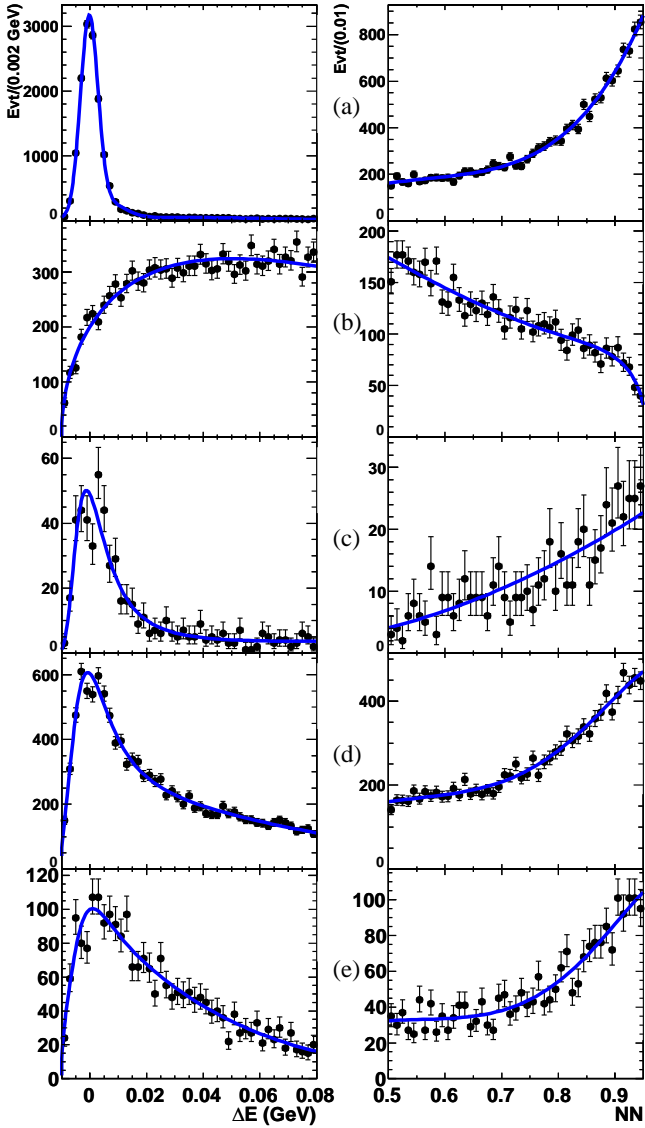


FIG. 6: Distributions of ΔE (left) and NN (right) for the five components of the fit: (a) $K_S^0 K_S^0 K_L^0$ signal, (b) combinatoric background, (c) $K_S^0 K_S^0 \pi^0$, (d) $K_S^0 K_S^0 K_S^0$, and (e) KKK^* . The combinatoric NN distribution is from the data sideband ($\Delta E > 0.010$ GeV). The rest of the distributions are from Monte Carlo samples.

fixed PDF parameters (2.6 events), our uncertainty on the fit bias correction (0.2 events), and the uncertainty on the charmonium background subtraction (1.1 events). The multiplicative contributions are from the uncertainties on the K_S^0 and K_L^0 reconstruction efficiencies (6.8 and 8.0%), the number of BB events in the sample (1.1%), and the $K_S^0 \rightarrow \pi^+ \pi^-$ branching fraction.

Figure 7 shows the fitted distributions of ΔE and NN , where a cut has been made on the fit variable not shown (e.g. there is a NN cut applied for the ΔE plot) to enhance the signal. The signal efficiency of this cut is 57%

for the ΔE distribution and 71% for the NN distribution.

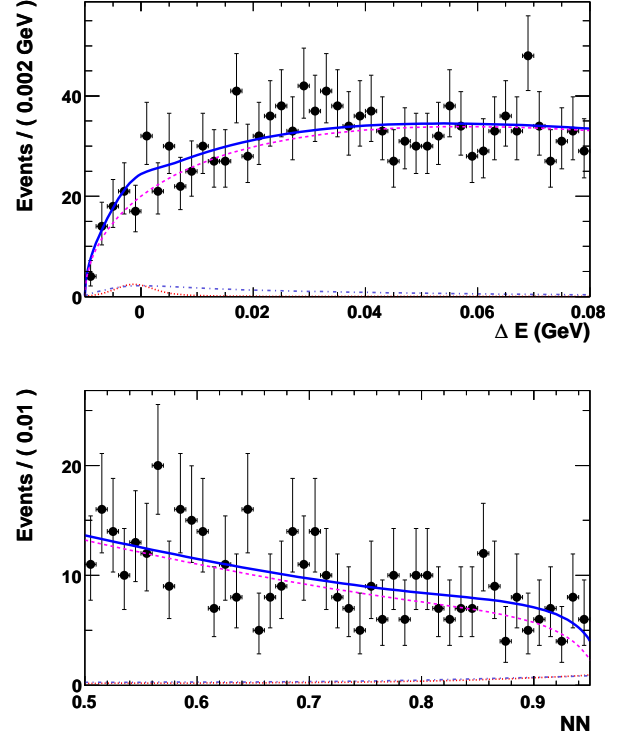


FIG. 7: Distributions of ΔE (top) and NN (bottom) for the $K_S^0 K_S^0 K_L^0$ fit. The plot of ΔE (NN) is for events passing a cut on NN (ΔE) which enhances the signal. The signal efficiency of this cut is 57% for the ΔE distribution and 71% for the NN distribution. The points with error bars are histograms of data samples. The solid curves are total PDFs. The dashed curves are combinatoric backgrounds. The dot-dashed curves are peaking B backgrounds. The dotted curves are signal PDFs.

The true distribution of $K_S^0 K_S^0 K_L^0$ events in the Dalitz plot is unknown. We use the average signal efficiency assuming a uniform true Dalitz distribution (8.1 %) to compute the $K_S^0 K_S^0 K_L^0$ branching fraction. We found no significant dependence of the signal ΔE resolution or the signal NN shape on the Dalitz plot variables. With these assumptions, we find a $K_S^0 K_S^0 K_L^0$ branching fraction, excluding the ϕ resonance, of $\mathcal{B}(B^0 \rightarrow K_S^0 K_S^0 K_L^0) = (2.4^{+2.7}_{-2.5} \pm 0.6) \times 10^{-6}$, where the first error is statistical and the second error is systematic. The dominant systematic error is from the uncertainties of peaking B backgrounds (23% relative).

Figure 8 shows a scan of the negative log likelihood as a function of the $K_S^0 K_S^0 K_L^0$ branching fraction, where the minimum negative log likelihood has been subtracted. In order to remove any dependence on our estimate of the total KKK^* branching fraction, we conservatively fix the KKK^* yield to zero in the scan of the log likelihood. We compute a one-sided Bayesian 90% confidence-level upper limit on the branching fraction assuming a

uniform prior probability for positive (physical) branching fraction values. Systematic errors are included by convolving the fit likelihood with a Gaussian distribution with a width corresponding to the total systematic error, excluding the uncertainty on the KKK^* yield, since it is fixed to zero in the likelihood scan. The result for the non-resonant three-body branching fraction is $\mathcal{B}(B^0 \rightarrow K_s^0 K_s^0 K_L^0) < 7.4 \times 10^{-6}$ at 90% C.L. Assuming the worst-case true Dalitz distribution, where the signal is entirely in the region of lowest efficiency (4%), the 90% C. L. upper limit on the branching fraction is 16×10^{-6} .

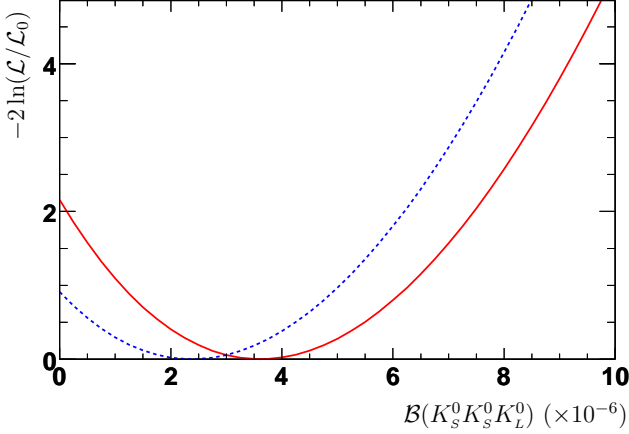


FIG. 8: Scan of the fit negative log likelihood as a function of the $K_s^0 K_s^0 K_L^0$ branching fraction, where the minimum negative log likelihood has been subtracted. A uniform true Dalitz distribution has been assumed for the $K_s^0 K_s^0 K_L^0$ signal. The solid curve includes the systematic uncertainty with yield of KKK^* fixed at 0 to calculate upper limit.

As a cross check on the analysis, we have performed the fit only in the ϕK_s^0 region of the Dalitz plot where the invariant mass of one of the $K_s^0 K_L^0$ pairs is less than $1.049 \text{ GeV}/c^2$. The results are given in the second column of Table I. We find $8.3^{+5.5}_{-4.5}$ signal events, which corresponds to a branching fraction of $\mathcal{B}(B^0 \rightarrow \phi K_s^0) = (4.0^{+2.6}_{-2.2}) \times 10^{-6}$, where the errors are statistical only. This is consistent with the world average value of $0.5 \cdot \mathcal{B}(B^0 \rightarrow \phi K^0) = (4.3^{+0.7}_{-0.6}) \times 10^{-6}$ [16].

We checked our estimation of the KKK^* peaking background yield by allowing it to float in the fit. This fit gave a KKK^* yield of -54 ± 170 events, which is consistent with our estimation of 70 ± 35 events.

V. SUMMARY

We have searched for the decay $B^0 \rightarrow K_s^0 K_s^0 K_L^0$ using 232 million $B\bar{B}$ pairs recorded by the BABAR experiment. We find no significant evidence for this decay. The central value for the branching fraction, assuming a uniform true Dalitz distribution for the signal and excluding the ϕ resonance, is $\mathcal{B}(B^0 \rightarrow K_s^0 K_s^0 K_L^0) = (2.4^{+2.7}_{-2.5} \pm 0.6) \times 10^{-6}$, where the first error is statistical and the second

TABLE I: Results of the fit for yields, branching fraction calculation, and branching fraction upper limit (UL) calculation. The $K_s^0 K_s^0 K_L^0$ efficiency below assumes a uniform true Dalitz distribution. The maximum likelihood fit bias and charmium background are subtracted from the signal yield branching fraction calculation.

Mode	$K_s^0 K_s^0 K_L^0$	ϕK_s^0
Events to fit	5892	210
Signal yield	$23^{+23}_{-22} \pm 6$	$8.3^{+5.5}_{-4.5}$
Comb. Bkg	5777 ± 79	202 ± 15
KKK^* Bkg	70 (fixed)	NA
$K_s^0 K_s^0 K_s^0$ Bkg	20 (fixed)	NA
$K_s^0 K_s^0 \pi^0$ Bkg	2.3 (fixed)	NA
Estimated fit bias (evt)	+0.3	0.0
$c\bar{c}K_{S/L}$	2.1	NA
MC ϵ (%)	8.7	6.1
K_s^0 corr. (%)	96.2	
K_L^0 corr. (%)	96.1	
Corr. ϵ (%)	8.1	5.6
$\prod \mathcal{B}_i$ (%)	47.5	16.2
Corr. $\epsilon \times \prod \mathcal{B}_i$ (%)	3.8	0.91
$\mathcal{B} (\times 10^{-6})$	$2.4^{+2.7}_{-2.5} \pm 0.6$	$4.0^{+2.6}_{-2.2}$
Stat. signif. (σ)	1.0	2.2
Signif. w/ syst. (σ)	0.9	
90% CL UL $\mathcal{B} (\times 10^{-6})$ (stat.)	6.3	NA
90% CL UL $\mathcal{B} (\times 10^{-6})$ (incl. syst.)	7.4	NA

error is systematic. This corresponds to a Bayesian 90% C.L. upper limit of $\mathcal{B}(B^0 \rightarrow K_s^0 K_s^0 K_L^0) < 7.4 \times 10^{-6}$. Assuming the worst-case true Dalitz distribution, where the signal is entirely in the region of lowest efficiency, the upper limit on the branching fraction is 16×10^{-6} . Our results show that the $K_s^0 K_s^0 K_L^0$ channel will be of limited use in understanding the $b \rightarrow s\bar{q}q$ penguin CP anomaly, due to the low efficiency times branching fraction, which limits the yield of signal events.

VI. ACKNOWLEDGMENTS

We are grateful for the extraordinary contributions of our PEP-II colleagues in achieving the excellent luminosity and machine conditions that have made this work possible. The success of this project also relies critically on the expertise and dedication of the computing organizations that support BABAR. The collaborating institutions wish to thank SLAC for its support and the kind hospitality extended to them. This work is supported by the US Department of Energy and National Science Foundation, the Natural Sciences and Engineering Research Council (Canada), Institute of High Energy

TABLE II: Estimates of systematic errors. Multiplicative systematic errors are in percent while additive systematic errors are in events. The fit yield systematic error is due to fixed fitting parameters, mainly from $K_S^0 K_S^0 K_L^0 \Delta E$ PDF parameters, and the uncertainties of fixed peaking B background yields. The fit bias error is one half of the bias. The $c\bar{c}K_{S/L}$ error is the uncertainty of charmonium background subtraction, estimated as one half of the subtraction.

Quantity	$K_S^0 K_S^0 K_L^0$
Additive errors (events)	
KKK^* normalization	5.2
Fit yield	2.6
Fit bias	0.2
$c\bar{c}K_{S/L}$	1.1
Total additive (events)	5.9
Multiplicative errors (%)	
K_S^0 efficiency	6.8
K_L^0 efficiency	8.0
Number $B\bar{B}$	1.1
$\mathcal{B}(B^0 \rightarrow K_S^0 \rightarrow \pi^+ \pi^-)$	0.4
Total multiplicative (%)	10.6
Total errors [$\mathcal{B}(10^{-6})$]	0.6

Physics (China), the Commissariat à l'Energie Atomique and Institut National de Physique Nucléaire et de Physique des Particules (France), the Bundesministerium für Bildung und Forschung and Deutsche Forschungsgemeinschaft (Germany), the Istituto Nazionale di Fisica Nucleare (Italy), the Foundation for Fundamental Research on Matter (The Netherlands), the Research Council of Norway, the Ministry of Science and Technology of the Russian Federation, and the Particle Physics and Astronomy Research Council (United Kingdom). Individuals have received support from CONACyT (Mexico), the Marie-Curie Intra European Fellowship program (European Union), the A. P. Sloan Foundation, the Research Corporation, and the Alexander von Humboldt Foundation.

-
- [1] M. Kobayashi and T. Maskawa, *Prog. Theor. Phys.* **49**, 652 (1973).
- [2] See, for example, D. Kirkby and Y. Nir in S. Eidelman *et al.*, Particle Data Group, *Physics Letters* **B592**, 1 (2004).
- [3] Y. Grossman and M. Worah, *Phys. Lett.* **B395**, 241 (1997).
- [4] (Belle Collaboration) K.-F. Chen *et al.*, *Phys. Rev.* **D72**, 012004 (2005), (BABAR Collaboration) B. Aubert *et al.*, *Phys. Rev.* **D71**, 091102(R) (2005), (BABAR Collaboration) B. Aubert *et al.*, *Phys. Rev. Lett.* **94**, 191802 (2005), (BABAR Collaboration) B. Aubert *et al.*, *Phys. Rev. Lett.* **94**, 041802 (2005), (BABAR Collaboration) B. Aubert *et al.*, *Phys. Rev.* **D71**, 111102 (2005), (BABAR Collaboration) B. Aubert *et al.*, *Phys. Rev. Lett.* **93**, 181805 (2004).
- [5] (BABAR Collaboration) B. Aubert *et al.*, *Phys. Rev. Lett.* **95**, 011801 (2005), (Belle Collaboration) A. Garmash *et al.*, *Phys. Rev.* **D69**, 012001 (2004), (Belle Collaboration) K. Sumisawa *et al.*, *Phys. Rev. Lett.* **95**, 061801 (2005).
- [6] For the most recent summary of all $b \rightarrow s\bar{q}q$ penguin CP asymmetry measurements, see the Heavy Flavor Averaging Group summary at <http://www.slac.stanford.edu/xorg/hfag/> and hep-ex/0603003.
- [7] H. Y. Cheng, C. K. Chua, and A. Soni, *Phys. Rev.* **D72**, 094003 (2005).
- [8] T. Gershon and M. Hazumi, *Phys. Lett.* **B596**, 163 (2004).
- [9] (Belle Collaboration) A. Garmash *et al.*, *Phys. Rev.* **D71**, 092003 (2005), (BABAR Collaboration) B. Aubert *et al.*, BABAR-PUB-06/006, hep-ex/0605003, submitted to *Phys. Rev. D*.
- [10] A preliminary Dalitz analysis of the decay $B^0 \rightarrow K^+ K^- K_S^0$ is given in (BABAR Collaboration) B. Aubert *et al.* BABAR-CONF-05/021, hep-ex/0507094.
- [11] M. Gronau and J. L. Rosner, *Phys. Rev.* **D72**, 094031 (2005).
- [12] BABAR Collaboration, B. Aubert *et al.*, *Nucl. Instrum. Methods*, **A479**, 1 (2002).
- [13] PEP-II Conceptual Design Report, SLAC-R-418 (1993).
- [14] A. Drescher *et al.*, *Nucl. Instrum. Methods*, **A237**, 464 (1985).
- [15] R. Sinkus and T. Voss, *Nucl. Instrum. Methods*, **A391**, 360 (1997), F. Zernike, *Physica* **1**, 689 (1934).
- [16] Particle Data Group, S. Eidelman *et al.*, *Physics Letters* **B592**, 1 (2004).
- [17] $f(x) \propto x\sqrt{1-x^2} \exp[-\xi(1-x^2)]$ with $x = (C + \Delta E_{\min} - \Delta E)/C$, $C = 5.29$ GeV or $x = NN/NN_{\max}$. See ARGUS Collaboration, H. Albrecht *et al.*, *Phys. Lett.* **B241**, 278 (1990).

